6.2 NCAR's NEW RAMAN-SHIFTED EYE-SAFE AEROSOL LIDAR (REAL)

Shane D. Mayor*, Scott M. Spuler, Jack R. Fox, Timothy D. Rucker, and Bruce M. Morley
Atmospheric Technology Division
National Center for Atmospheric Research
Boulder, Colorado

1. INTRODUCTION

Scanning lidar measurements in urban areas are becoming more important for reasons associated with the impact of aerosol emissions on climate and issues related to homeland security. In particular, scanning aerosol backscatter lidars offer the ability to detect, map, and track plumes of potentially hazardous aerosols. Because urban areas are crowded with people, buildings, and air traffic, eye-safety is imperative.

Many other lidars already exist and many of them are eye-safe (for examples, Spinhirne 1993 and Grund et al. 2001). So, why did NCAR create REAL and why is it unique? REAL transmits relatively high energy pulses (>200 mJ/pulse) when compared to other systems and yet remains eye-safe at all ranges. It produces high signal-to-noise ratio aerosol backscatter from individual laser pulses and provides high range resolution (3 m) data. Therefore, REAL is quite different from existing micropulse and coherent Doppler lidar systems.

2. EYE-SAFETY

No optical wavelength is inherently eye-safe, but some wavelengths are safer than others. This is reflected in figure 1. It shows the maximum eye-safe energy for a pulsed laser as a function of beam wavelength. The chart shows that the region between 1.5 and 1.8 microns allows the transmission of the highest permissible energy. This is due to the volumetric absorbing capability of the fluid of the eye. With modest beam expansion (i.e. distributing the pulse energy over a larger beam diameter) it is possible to safely transmit over 1 J per pulse in this region. REAL's transmit beam diameter is approximately 5 cm at the exit aperture.

* Corresponding author address: Dr. Shane D. Mayor, NCAR, P.O. Box 3000, Boulder, CO 80307-3000, 303-497-2037, e-mail: shane@ucar.edu

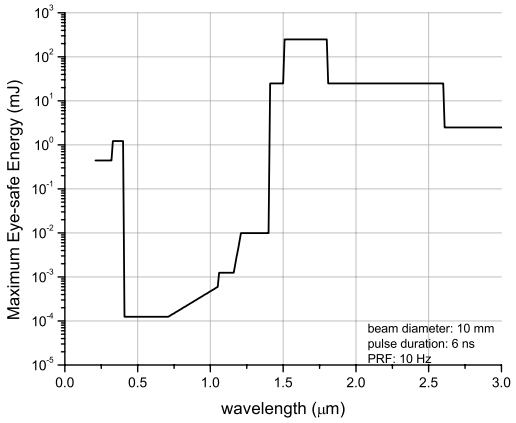

Figure 1: Maximum eye-safe energy as a function of wavelength for a 10 mm diameter beam, 6 ns pulse duration, and 10 Hz pulse repetition frequency.

3. PRINCIPLES OF OPERATION

REAL employs a multi-pass gas cell filled with 10 atmospheres of pure methane to convert 1.0 micron wavelength Nd:YAG laser light to the safer 1.54 micron wavelength by stimulated Raman scattering. Although REAL uses Raman scattering in its transmitter as its name implies, it is not a "Raman lidar" such as the system described by Whiteman et al. (1992) which detects inelastic scattering from water vapor in the atmosphere. In contrast, REAL uses Raman scattering in the transmitter's methane cell to generate light in the wavelength region with highest maximum permissible exposure. REAL detects elastically backscattered light from small particles in the atmosphere. Therefore, REAL is not a "Raman Lidar" in the traditional sense of the name.

4. FIRST RESULTS

We operated REAL from the NCAR Foothills Laboratory from May through October of 2003 in a vertical stare mode. Initially, we transmitted the non-eye-safe 1.0 micron wavelength beam simultaneously and coaxially with the eye-safe 1.5 micron beam in order to compare backscatter from the two wavelengths (see

Figure 3). Nd:YAG lasers operating at 1.0 micron and high performance silicon detectors are robust and commercially available, therefore operation at this wavelength is relatively straightforward. Transmitting 1.0 micron light simultaneously enabled performance verification of the relatively unexplored wavelength of 1.5 microns. When operating with the non-eye-safe beam, we employ a vertically pointing 3-cm Doppler radar (Gray and Pratte, 2003) to provide a microwave cone around the laser beam. Aircraft entering the microwave region are detected by the radar and the laser is instantly turned off. Figure 3 demonstrates that it is possible to resolve important microscale detail at 1.54 microns wavelength. The top image appears smoother because of the slower electronics in the receiver of the 1.54 micron channel. The electronics were upgraded to provide equivalent range resolution prior to achieving the scanning capability presented in the next section.

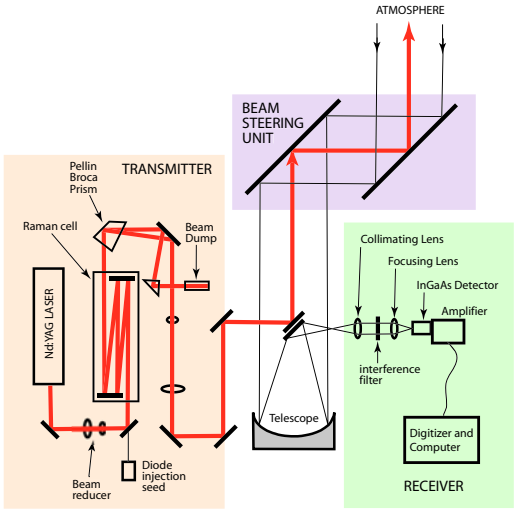

Figure 2: System schematic of REAL.

Characteristic	Value
Wavelength (nm)	1543
Transmit energy (mJ/pulse)	220
Pulse repetition frequency (Hz)	10
Pulse duration (ns FWHM)	4
Diameter of transmit beam (cm)	5
Telescope diameter (cm)	40
Analog-to-digital sample rate (MHz)	50
Analog-to-digital resolution (bits)	14
Divergence of transmit beam (full, mrad)	0.48
Field-of-view of receiver (full, mrad)	0.54
Receiver filter bandwidth (nm)	5
Detector diameter (mm)	0.2

Table 1: REAL system specifications.

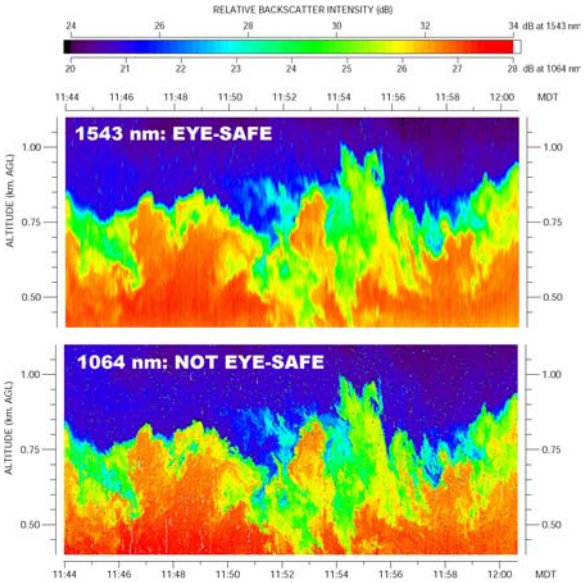

Figure 3: Time-versus-height of relative aerosol backscatter from 400 m to 1100 m above the ground and over a 17-minute period on 10 July 2003 in Boulder, Colorado. These data showing the structure of the entrainment zone of a convective boundary layer have a temporal resolution of 1 s and a vertical resolution of 50 m (top) and 3 m (bottom).

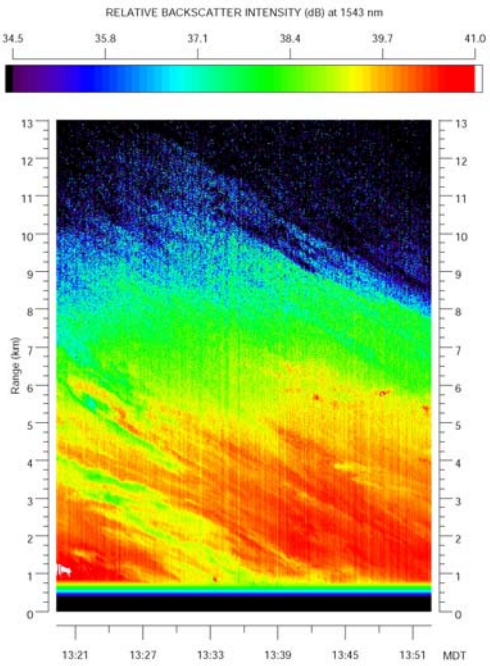

Figure 4: Time-versus-range of aerosol backscatter at 1.54 microns for a 33-minute period on 18 July 2003. The laser beam was stationary and pointed in an almost horizontal position (3-degrees above the horizon) during this period.

5. First Scanning Field Demonstration

Based on the promising lab demonstrations presented in section 4, we designed and built a beam steering unit to add scanning capability. We installed REAL and the new beam steering unit in a 20x8x8 ft standard shipping container and collected our first scanning data in May of 2004 in the downtown of a major city. Figures 5 through 7 are examples of the types of scan images REAL is capable of providing. In all three scan images, no temporal averaging was applied to the data. In other words, each ray was the result of backscatter from a single pulse. REAL operated at 10 Hz obtain these figures. PPI sector scans such as figures 5 and 7 took approximately 20 s to obtain. In figure 5, we can see the detailed spatial structure of aerosol plumes on a horizontal scan plane in the lowest 100 meters of the atmosphere. Animation of the images provides information about the advection of the plumes. Derivation of vector wind fields was recently described by Mayor and Eloranta (2001) from similar data. Additional applications of scanning aerosol backscatter data include testing large eddy simulations (Mayor et al., 2003).

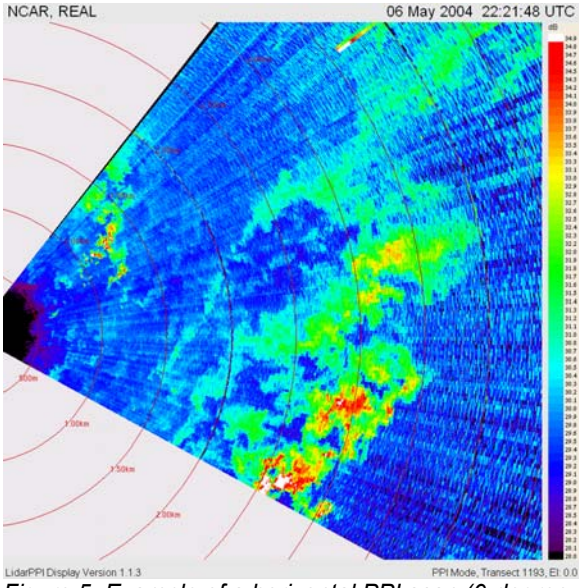

Figure 5: Example of a horizontal PPI scan (0-degree elevation angle) collected by REAL

Figure 7 shows a cloud-free gust-front approaching from the north with high aerosol scattering behind the sharp leading edge of the front. Observers at the REAL site noticed a wind shift and barely perceptible reduction of visibility when this feature arrived at the site. Figure 7 is also useful in answering the common question “How far can REAL see?” It shows that when aerosol scattering is strong, REAL can detect aerosol structures from over 10 km away. The radial strips in figure 7 are the result of variability in atmospheric attenuation and systematic electronic noise in REAL’s receiver subsystem. We are currently working to stabilize the electrical power supplied to the receiver for cleaner images in the future.

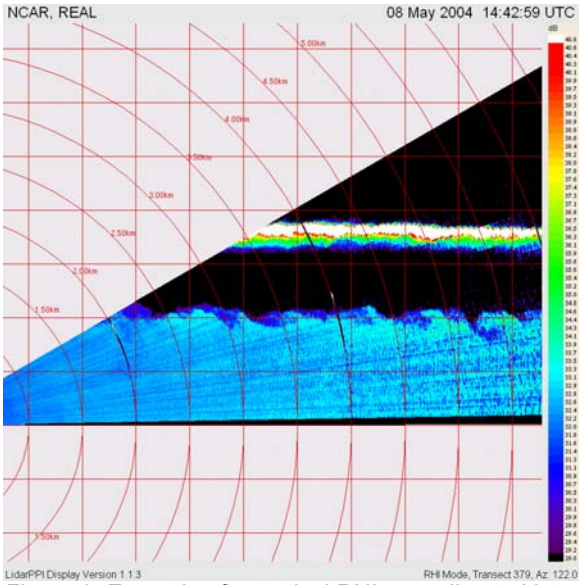

Figure 6: Example of a vertical RHI scan directed into the wind. The image shows a 1 km deep boundary layer with patterns resembling Kelvin-Helmholtz billows in the entrainment zone. Another high-scattering aerosol layer is detected at 1.75 km altitude.

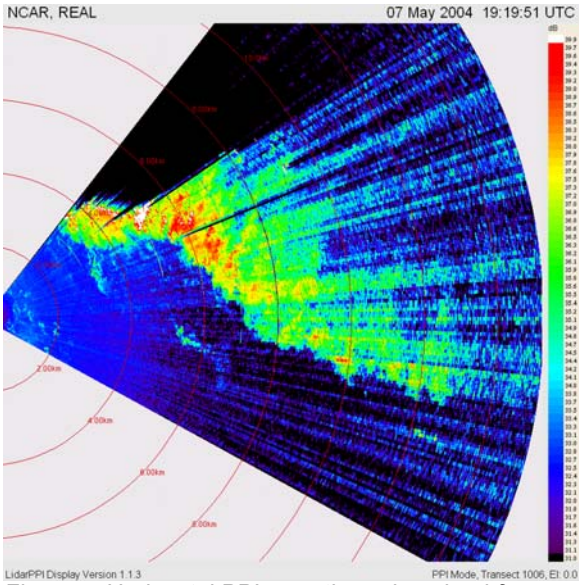

Figure 7: Horizontal PPI scan through a cloud-free gust front detected by REAL. The airmass behind the front had increased aerosol scattering and observers noted a sudden increase in surface wind speeds when it passed.

6. SUMMARY

A new, eye-safe, scanning, aerosol backscatter lidar was recently developed at NCAR and is available for use by the boundary layer research community. Interested researchers may read more about requesting NCAR observing facilities at www.atd.ucar.edu. More information about REAL is available at www.lidar.ucar.edu.

REFERENCES

Gray, G. R. and F. Pratte: 2003: An eye-safety radar for lidar operations, In AMS 31st International Conf on Radar Meteorology, Page P5B.9, Boston.

Grund, C. J., R. M. Banta, J. L. George, J. N. Howell, M. J. Post, R. A. Richter, and A. M. Weickman, 2001: High-resolution Doppler lidar for boundary layer and cloud research. *J. Atmos. Ocean. Tech.*, **18**, 376-393.

Mayor, S. D. and E. W. Eloranta, 2001: Two-dimensional vector wind fields from volume imaging lidar, *J. Appl. Meteor.*, **40**, 1331-1346.

Mayor, S. D., G. J. Tripoli, E. W. Eloranta, 2003: Evaluating large-eddy simulations using volume imaging lidar data, *Mon. Wea. Rev.,* **131**, 1428-1452.

Mayor, S. D. and S. M. Spuler: 2004: Raman-shifted Eye-safe Aerosol Lidar (REAL), *Appl. Optics*, **43**, To appear in 1 July issue.

Mayor, S. D., S. M. Spuler, and B. M. Morley: 2004: NCAR's New Raman-shifted Eye-safe Aerosol Lidar (REAL). 22nd International Laser Radar Conference. 12-16 July, Matera Italy.

Spinhirne, J. D., 1993: Micro pulse lidar*, IEEE Trans. Geosci. Remote Sens.*, **31**, 48-55.

Whiteman, D. N., S. H. Melfi, and R. A. Ferrare, 1992: Raman lidar system for the measurement of water vapor and aerosols in the Earth's atmosphere, *Appl. Optics*, **31**, 3068-3082.